

## NbZr multilayers. I. Structure and superconductivity

W. P. Lowe

*Department of Physics, Stanford University, Stanford, California 94305*

T. H. Geballe

*Department of Applied Physics, Stanford University, Stanford, California 94305  
and Bell Communications Research, Inc., Murray Hill, New Jersey 07974*

(Received 18 April 1983; revised manuscript received 1 August 1983)

Multilayers of NbZr have been made by the process of magnetron sputtering. The samples were prepared with modulation wavelengths  $\Lambda$  ranging from 200 Å down to 4 Å. The structural properties have been studied using x-ray scattering. The composition wave constructed from the x-ray scattering shows that the as-deposited square wave is not square but rather the Zr component has partially diffused into the Nb component. The Zr is believed to substitute on Nb sites and expand the lattice constant of the Nb layer. The compositional amplitude increases above  $\Lambda=31$  Å and decreases below  $\Lambda=31$  Å. A composition modulation was detected by x-ray scattering as low as  $\Lambda=13$  Å. Above  $\Lambda \geq 31$  Å the Nb is bcc with the [110] along the growth direction and the Zr is hcp with the [002] along the growth direction. The  $T_c$  in this region decreases linearly as  $\Lambda$  increases. In the region  $\Lambda \leq 31$  Å the Zr undergoes a structural phase transition to form a bcc lattice that is coherent with the Nb lattice. Once the multilayer becomes coherent there is a sharp increase in the superconducting transition temperature with decreasing  $\Lambda$ . This increase in  $T_c$  approaches 9.7 K which is the value for a 50 at. % solid solution of NbZr. A trilayer model is applied in the Cooper limit to explain the critical temperatures. This model implies a superconducting coherence length of approximately 100 Å.

### I. INTRODUCTION

Metallic multilayers have been produced over the last few years by sputtering and electron-beam evaporation with varying degrees of success. The structure of multilayers such as CuNi,<sup>1</sup> NbCu,<sup>2,3</sup> NbTa,<sup>4,5</sup> and NbTi (Ref. 6) has been mostly worked out by x-ray scattering and is understood to a large degree at present. The current interest in these and other multilayers is what effects are impressed on other physical properties by the novel arrangement of the atoms. This is a question that of course cannot be given a general answer. At present an in-depth study of different multilayer systems are of value. Unlike the equilibrium systems to which they are related there are questions as to how the constituents will react once they are sequentially deposited. The multilayering of some elements together has been unpredictable. Therefore the initial characterization should be to determine the structure of the multilayer. In this work we have done detailed x-ray scattering to study long-range atomic correlations. For the first time, extended x-ray-absorption fine structure (EXAFS) (results reported in next paper) has been performed on companion samples in order to study the local atomic environment (see Ref. 7).

Niobium and zirconium form a continuous disordered solid solution in which the superconducting transition temperature is strongly composition dependent and can be as high as 11 K. Studies have been made of the superconducting properties over a wide composition range with emphasis on the composition Nb<sub>0.75</sub>Zr<sub>0.25</sub> where the maximum  $T_c$  occurs and where also some evidence for phonon

softening has been reported.<sup>8</sup> Tunneling studies have also been done to probe the density of states at this composition.<sup>9</sup>

As for the structural properties much work has been done with respect to the  $\omega$ -phase lattice instability which occurs at a composition different from that of maximum  $T_c$ .<sup>10,11</sup> The  $\omega$  longitudinal distortion wave manifests itself predominantly along the [111] direction in the bcc lattice, producing sharp or diffuse (depending on the composition of the alloy) superlattice reflections.<sup>12</sup>

With the above information available for the NbZr solid solution, novel properties brought about by the superperiodicity of the NbZr multilayer should be recognizable. Since Nb and Zr form a solid solution they are likely to form a coherent interface which should provide a better sample for some of the low-temperature measurements that require fairly long mean free paths. In this article we describe results from x-ray scattering and  $T_c$  measurements both above and below the point at which the lattice becomes coherent.

### II. SAMPLE PREPARATION

The multilayers were prepared by magnetron sputtering.<sup>13</sup> With this technique a variety of multilayers can be made quite conveniently and quickly. The modulation wavelength ranged from  $\Lambda=4$  to 200 Å for this set of samples. The samples were made on room-temperature sapphire substrates with (1 $\bar{1}$ 2) orientation for use in this research, and simultaneously on kapton for EXAFS studies reported in the following paper. Sputtering rates were

between 10 and 20 Å/sec in an argon pressure of  $2 \times 10^{-3}$  Torr. The initial pressure of the vacuum chamber was  $5 \times 10^{-6}$  Torr. Each sample was roughly 1  $\mu\text{m}$  in total thickness. The rates were set such that the thickness of the Nb would be equal to that of the Zr and each layer would contain an integral number of atomic layers. Microprobe analysis of the samples showed a spread in Nb composition of 10 at. % with the mean Nb composition being 51 at. %. As has been found previously, when layering other elements there was satisfactory agreement (to within 4%) between the multilayer period determined by diffraction and that calculated from the deposition parameters.<sup>13</sup>

### III. STRUCTURE OF NbZr MULTILAYERS

The quality of a multilayer has to be considered from two perspectives: Firstly, the crystalline perfection of the individual layers which also includes the interfaces between the different species, and secondly, the atomic plane stacking along the growth direction. The multilayers are textured along the growth direction, giving rise to vastly differently scattering patterns for different directions in reciprocal space. With the scattering vector along the growth direction, only the planar correlation along the growth direction contributes to the scattering. When the scattering vector is at some angle  $\eta = 90 - \chi$  to the growth direction, the planar correlation in the Nb and the Zr produces separate and distinct scattering patterns in reciprocal space; therefore we consider each direction separately.

#### A. When $\eta \neq 0$

In this case  $\vec{q}$  is not along the growth direction and the Nb and Zr have separate and distinct scattering patterns in reciprocal space. Longitudinal scans in reciprocal space were made along high-symmetry directions, i.e.,  $\eta = 30^\circ$ ,  $45^\circ$ , and  $60^\circ$ . The two diffraction patterns can be separated, and, in practice, can be indexed to obtain lattice constants and orientations for the Nb layers and the Zr layers. The two different patterns also reflect the hcp symmetry for Zr and the bcc symmetry for the Nb. By scattering in this geometry, the degree of crystalline order of the individual layers can be determined in a straightforward manner, in that complicated scattering effects due to the multilayer periodicity essentially do not contribute to the scattered intensity. Several peaks from each lattice were recorded and analyzed to give crystallographic orientation, lattice constant, and an estimate of apparent grain size.

Most multilayers sputtered onto unheated substrates will form with the closed-packed planes of each constituent stacked along the growth direction. When  $\Lambda \geq 31$  Å, this is also the case for NbZr multilayers, in that reflections could be indexed from each lattice that by symmetry would require the [110] direction of Nb and the [002] direction of Zr to be normal to the substrate. The mosaic spread in the diffracting domain with respect to the substrate normal is given by the width of  $\eta$  and for these samples was  $\Delta\eta \approx 5^\circ$  full width at half maximum (FWHM) when  $\Lambda \geq 31$  Å.

With the use of the separate reflections from each of the layers, different lattice constants can be distinguished

for both Nb and Zr. In general, as  $\Lambda$  is decreased, the lattice constant of Nb increases from its bulk value of 3.30 Å to approximately 3.40 Å at  $\Lambda = 51$  Å. The scattering pattern of the Zr layers can be indexed as hcp with average lattice constants of  $a_0 = 3.24$  Å and  $c_0 = 5.21$  Å for  $\Lambda \geq 109$  Å.

Within the region of modulation wavelength,  $109 \leq \Lambda \leq 51$  Å, the Zr lattice undergoes a gradual phase transition from hcp to bcc. Once obtaining the Zr bcc phase only one bcc lattice is present within the multilayer structure. The bcc Nb lattice tends toward forming coherent interfaces with the bcc Zr lattice. This can be seen in the x-ray scans where  $\eta = 45^\circ$  [Fig. 1(a)] in which

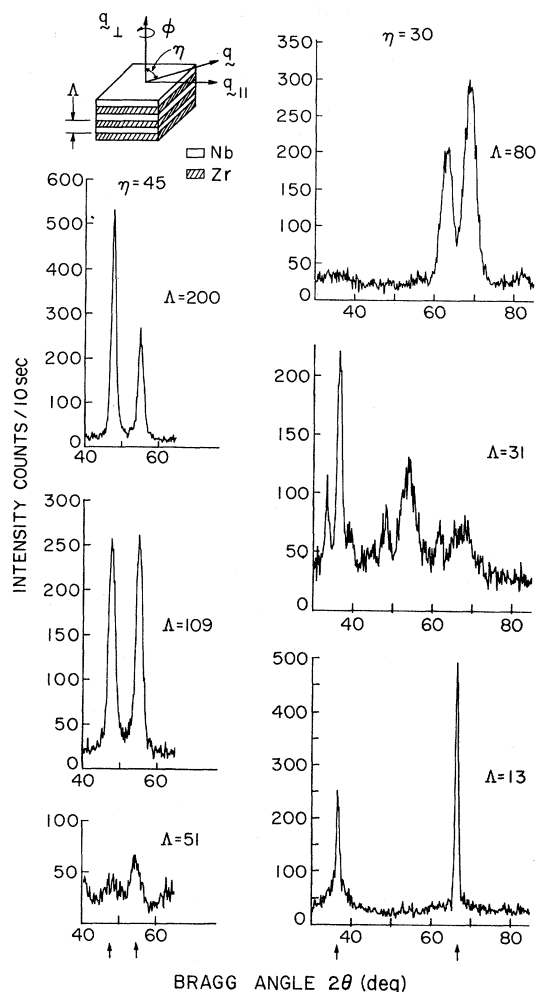


FIG. 1. Longitudinal scans along two directions in reciprocal space ( $\eta = 45^\circ$  and  $30^\circ$ ) showing the intralayer crystalline structure of the multilayer as the modulation wavelength is decreased. In scans with  $\eta = 45^\circ$ , Zr(102) and Nb(200) is seen to decrease as  $\Lambda$  decreases, indicating the diminishing hcp Zr phase. The appearance of hcp peaks in the  $\eta = 30^\circ$  scans for  $\Lambda = 80$  Å indicate that at this modulation wavelength the Nb and Zr lattices are incoherent. However, the hcp Zr undergoes a structural transition to bcc Zr in the neighborhood of  $\Lambda = 31$  Å, and forms a coherent interface with the Nb layers resulting in one bcc lattice. Zr(102), Nb(200), NbZr(101), and NbZr(211) are indicated, respectively, by the arrows.

the hcp Zr(102) reflection decreases to almost zero when  $\Lambda$  reaches 51 Å. The intensity of the Nb(200) reflections also shows a large sudden decrease at  $\Lambda=51$  Å. These large decreases in intensities are accompanied by slight shifts (larger for Nb) in the peak positions. In this Zr transition region the intensity of the hcp Zr peaks are diminished. The Zr phase transition probably starts at the Nb-Zr interfaces where randomly oriented islands of bcc Zr are formed and surrounded by hcp Zr. Within this two-phase region ( $\alpha$ - and  $\beta$ -Zr) a few hcp reflections can still be measured; however, due to their small numbers and very weak peak intensities lattice constants could not be calculated. The weak reflections were also investigated unsuccessfully with respect to the  $\omega$  phase. It was also noted that the Nb, although maintaining its orientation and bcc lattice character throughout the Zr transition, also showed decrease peak intensities. This suggests that the Nb crystallites are becoming more random within the layers.

Below  $\Lambda=31$  Å the Zr transition is complete and x-ray scans with  $\eta=30^\circ$  show the emerging single bcc lattice [Fig. 1(b)]. The peak intensity shows a significant increase and the peak width has decreased significantly. The new bcc lattice has a lattice constant of  $a_0=3.44$  Å at  $\Lambda=4$  Å. The reported lattice constant for the bcc NbZr solid solution is 3.454 Å. The lattice is oriented with the [110] direction normal to the substrate and  $\Delta\eta\leq 2^\circ$  FWHM, which is less than half of the mosaic spread of the larger- $\Lambda$  samples. Whether or not the sample remains layered at this point cannot be determined in the  $\eta\neq 0$  geometry; however, evidence will be presented in the next section to show that a large degree of modulation remains.

The scattering intensity of all the peaks (both for Nb and Zr when  $\Lambda\geq 51$  Å) is independent of  $\phi$ , the azimuthal angle in reciprocal space, and therefore, over the area of the incident beam ( $1\times 6$  mm<sup>2</sup>), there are a large number of grains with random orientation in the plane of the layers. This is also characteristic of many of the other multilayer systems sputtered on unheated substrates.

In considering contributions to the diffraction peak width with respect to the multilayers it is necessary to differentiate between coherent interfaces and long-range planar correlation. When an interface is coherent there is an atomic translation vector that connects atoms across that interface, i.e., in the case of coherent domains of NbZr multilayers there is one lattice within the diffracting domain. Coherent interfaces are accompanied by long-range planar correlation, or, more specifically, the atomic planes in, for instance, one Nb layer, have the same atomic spacing and orientation as the planes in the Nb layers above and below it. (It is possible to obtain such a long-range planar correlation without coherent interfaces; however, a likely candidate for this type of behavior are NbCu multilayers in which the interfaces are incoherent and the modulation wavelengths can be made very small, but no such long-range correlations were observed.) The diffraction-peak width is then related to the correlation length  $t_{hkl}$  by the Scherrer equation<sup>14</sup> where  $B(2\theta)$  is the added width of the peak,

$$t_{hkl} = \frac{0.9\lambda}{B(2\theta)\cos\theta} \quad (1)$$

and  $\lambda=1.542$  Å, the weighted average Cu  $K\alpha$  x-ray wavelength. The grain size or the atomic correlation length as given by the Scherrer equation is inversely related to the width of the diffraction peak. The peak width is related to the number of planes that satisfy the diffraction condition independent of whether or not the planes are in contiguous regions. If the intensity contributions to the diffraction peak are from noncontiguous crystalline regions that have the same crystallographic orientation and the regions are separated by an integer number of plane spacings, then the width of the peak, according to the Scherrer equation, will be represented by the planes within all the noncontiguous regions. This condition is much more likely in multilayers than in alloys, and thus an apparent grain size or apparent correlation length is obtained from the peak width in a multilayer. This condition is always present for scattering along the growth direction ( $\eta=0$ ) and provides a substantial contribution to the very narrow x-ray peaks, as in the case of NbCu.<sup>2</sup>

To obtain the intrinsic width of the sample diffraction peaks, the peak width of a Si standard was first measured to obtain the instrumental broadening and then used in the following equation:

$$B^2(2\theta) = B_{\text{expt}}^2 - B_{\text{stan}}^2 \quad (2)$$

where  $B_{\text{expt}}$  is the width of the sample peak and  $B_{\text{stan}}$  is the width of the standard's peak. The Si standard has a grain size greater than 2000 Å; thus instrumental broadening could be removed using Eq. (2). No corrections were made for strain broadening of the diffraction peaks, thereby attributing the entire added peak width to particle size. Therefore the apparent grain sizes represent a lower limit with respect to particle size.

The apparent correlation length for the NbZr multilayers where  $200\geq\Lambda\geq 109$  Å is approximately 800 Å where the apparent correlation length of Zr appears slightly longer than that of Nb. The apparent correlation length increases as  $\Lambda$  is decreased, more slowly in the transition region  $109\geq\Lambda\geq 51$  Å than in the coherent region  $\Lambda\leq 51$  Å. When  $\Lambda\leq 31$  Å the apparent correlation length in all directions is larger than 1000 Å. As is expected, the correlation length for NbZr increases as the interfaces become coherent.

#### B. When $\eta=0$

The multilayer stacking itself provides the major contribution to the scattered intensity in this geometry. Therefore the form and amplitude of the composition modulation are obtained in this scattering geometry. It should be noted that because the apparent correlations are much longer in this direction than when  $\eta\neq 0$ , the scattering intensity is much stronger and the peak width is smaller. Approaching the case of  $\vec{q}=\vec{q}_{||}$ , or looking parallel to the growth direction, the scattering patterns for  $\Lambda\geq 31$  Å show strong maxima surrounded by several orders of satellites [Fig. 2(a)]. The satellites are present due to a chemical modulation along the scattering direction. The effect of the chemical modulation is usually a modulation in  $d$  spacing and the intrinsic modulation of the scattering power. The form factor for a multilayer at position  $|\vec{q}|$

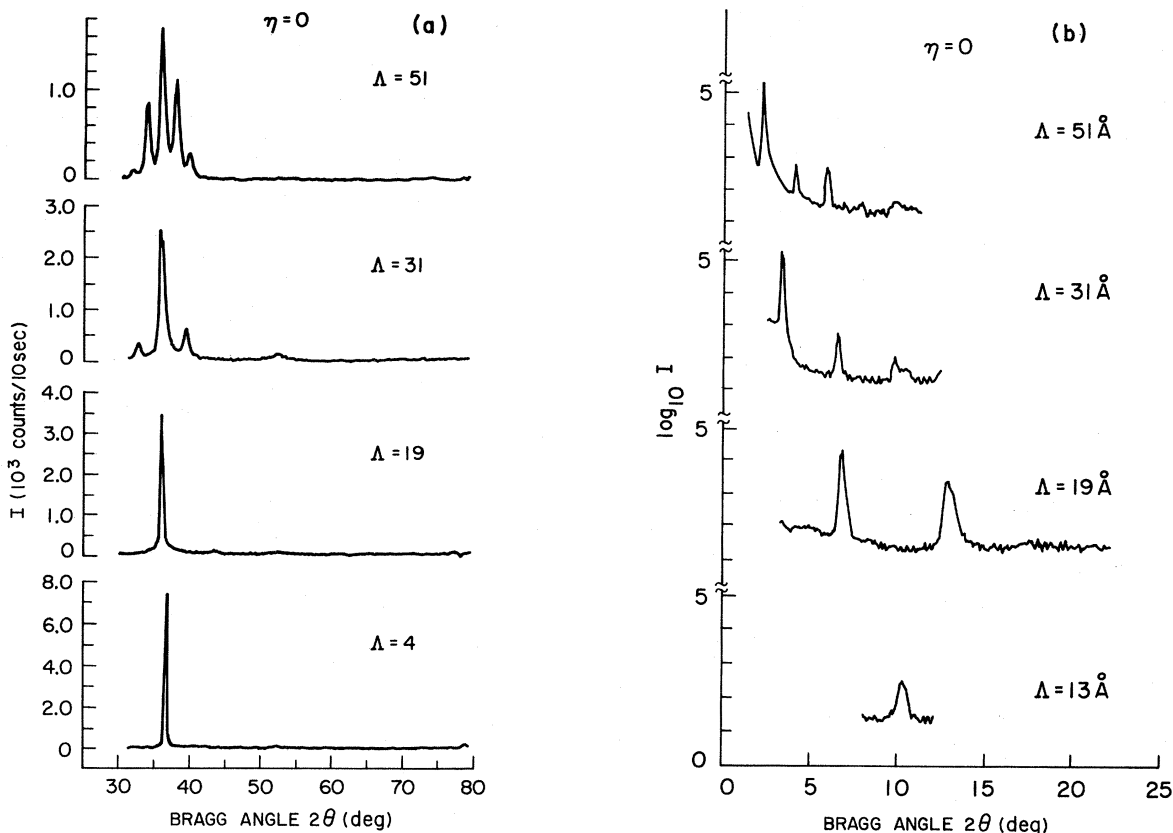


FIG. 2. (a) Scattering along the growth direction shows satellites when  $\Lambda \geq 31 \text{ \AA}$ . The main Bragg peak grows in intensity and atomic correlation length increases. It should be noted that although the satellites around the main peak in the  $\Lambda = 19 \text{ \AA}$  scan do not appear, this does not necessarily mean this sample has no composition modulation. (b) The positive satellites around the zero node were used to calculate the composition amplitude. The weak- (even-) order satellites appear in all samples where  $\Lambda \leq 51 \text{ \AA}$ , indicating that the composition modulation is not symmetric. Superlattice peaks can be seen for modulation wavelengths as small as  $\Lambda = 13 \text{ \AA}$ .

in reciprocal space, which is proportional to the scattered x-ray intensity, is then given by

$$f(\vec{q}) = \sum_{n=0}^{N-1} f_n e^{i\vec{q} \cdot \vec{r}_n}, \quad (3)$$

where  $f_n$  is the scattering factor of plane  $n$ , and  $\vec{r}_n$  reflects the separation between any two consecutive planes. In general, for a multilayer, both  $f_n$  and  $\vec{r}_n$  can be expressed in separate but related Fourier series.

Both the scattering-factor modulation and the plane-spacing modulation contribute to the amplitude of the satellites as stated by Eq. (3); however, when  $\vec{q}$  is small the contribution to the amplitude of the satellites is due almost totally to the scattering-factor modulation. Therefore if the zero-node satellites are used in Eq. (3), the exponential can be approximated by unity. In using the zero-node satellites we have neglected the small-strain contribution to their intensity. When the interfaces become coherent through a diffusion mechanism, the coherence strains are very small, if not zero, thus giving a very small exponent in Eq. (3) when the product is taken with  $|\vec{q}|$ . Therefore in this type of coherent system essential-

ly no error is introduced into the composition profile by neglecting strain for very small  $\Lambda$ . The composition profile or chemical modulation can then be related to the planar scattering factor by

$$f_n - \bar{f} = (f_{\text{Zr}} - f_{\text{Nb}})(c_n^{\text{Zr}} - c_0^{\text{Zr}}), \quad (4)$$

where  $f_{\text{Zr}, \text{Nb}}$  is the atomic scattering factor for Zr and Nb, respectively,  $c_n^{\text{Zr}}$  is the normalized fractional Zr atomic concentration in the  $n$ th and average plane, respectively, and  $\bar{f}$  is the atomic scattering factor of a plane with average composition ( $c_0$ ). The scattering factors are per atomic area to reflect the different atomic sizes and symmetry of the Nb and Zr planes. Then the composition of the multilayers can be written directly as a Fourier series,

$$c_n^{\text{Zr}} - c_0^{\text{Zr}} = \sum_{L=1}^M a_L \cos \frac{2\pi}{\Lambda} n d L, \quad (5)$$

where the Fourier coefficients are  $a_L$ , and  $d$  is the average spacing of the Nb and Zr planes along the growth direction. From the absolute scattering intensity of the satellites around the origin in reciprocal space, it can be shown

that the relationship between the scattered intensity and the Fourier coefficients is

$$a_L = \frac{2}{f_{\text{Zr}} - f_{\text{Nb}}} [I_L(q)]^{1/2}, \quad (6)$$

where  $I_L(q)$  is the absolute scattered intensity of the  $L$ th satellite.<sup>15</sup>

The spectrum of the zero-node satellites for  $51 \leq \Lambda \leq 13$  Å [Fig. 2(b)] were measured and corrected for polarization, geometrical, and temperature factors. The temperature correction was made by assuming an alloy of  $\text{Nb}_{0.5}\text{Zr}_{0.5}$  to obtain  $2B = 1.3 \text{ \AA}^2$ . The absorption was calculated using  $\bar{\mu}$ , the average linear absorption coefficient for Nb and Zr. Edge effects are small and were neglected in the calculation. The surprisingly intense satellites for such a small difference in atomic scattering factor is not due to anomalous scattering. The anomalous component of the atomic scattering factor for Nb and Zr is small, with  $\lambda/\lambda_K \approx 0.5$ , where  $\lambda_K$  is the wavelength of the respective Nb and Zr  $K$  absorption edges.

The composition modulation as determined from the zero-node satellites is shown in Fig. 3. The composition amplitude for  $\Lambda = 51$  Å was assumed to be 100 at. % Zr, and the amplitudes for samples with  $\Lambda < 51$  Å were normalized with respect to this sample. It is reasonable to assume that when  $\Lambda = 51$  Å there will be at least some planes of pure Zr in the Zr layer. The composition profiles are given in Fig. 3 for samples with  $\Lambda < 51$  Å. The relative sign of the coefficients have all been set in phase to give the maximum possible composition amplitude. The composition profiles are predominantly sinusoidal and decrease in amplitude as  $\Lambda$  decreases. Since the samples were made with an equal thickness of Nb and Zr, a compositional variation in the form of a square wave would only yield odd Fourier terms with many high-frequency components. In a system such as NbZr where a solid solution is formed, the interfaces are very likely to be smooth and probably broad, and therefore the compositional profile will not contain the high-frequency terms. This is the case for NbZr multilayers as evidenced by the

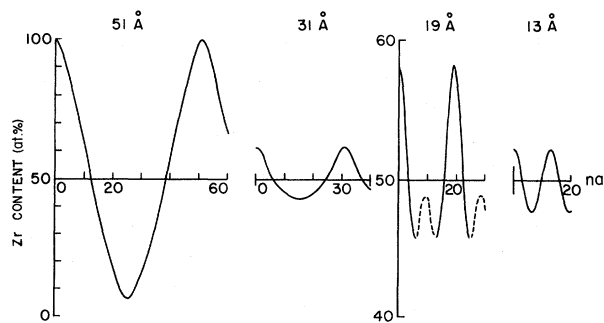


FIG. 3. Composition modulation calculated from the Fourier coefficients obtained from the satellite intensity in Fig. 2(b). The slight asymmetry in the composition indicates that there is preferential diffusion of Zr atoms into the Nb layers. The amplitudes have been normalized to 100 at. % Zr in the  $\Lambda = 51$  Å sample.

weak intensity of the higher-order satellites. Interfacial diffusion causes the composition amplitude to decrease and the interface to spread out as  $\Lambda$  decreases. There has been no observed decrease in the satellite intensity over a period of months, in which the initial measurement was made immediately after deposition, and therefore the diffusion must take place during deposition. The appearance of even-order satellites indicates that this diffusion has a net atomic migration across the interface. Since all of (even and odd) the higher-order satellites are quite weak relative to the  $L = 1$  satellite, there is very little measured effect on the symmetry of the composition profile.

The choice of the composition phase was made on the basis that the average lattice constant of the Nb layers showed a substantial increase at long modulation wavelengths. This indicates that there is net diffusion across the interface and that the Zr is most likely diffusing into the Nb, thus expanding the Nb lattice constant and giving the square composition wave a rectangular deviation. Reported lattice constants for NbZr solid solutions as a function of the percentage of Zr (Ref. 16) would indicate unrealistically high concentrations of diffused Zr if the measured lattice constant of the Nb layer were attributed solely to a solid solution. Therefore, as stated earlier, a substantial part of Nb lattice increase must be due to lattice strain caused by close proximity to the Zr layer. The lattice constant over the large- $\Lambda$  region, however, should not respond to strain from the Zr, especially if the interfaces are incoherent.

An independent determination of the phase of the composition wave could be made in order to verify the net direction of the atomic migration. An ideal way to determine the profile of the Nb- and Zr-rich regions would be a sputter depth probe with a chemical analyzer, but the depth resolution on all such probes is, at best, 10 Å, which would not be sufficient in the cases of  $\Lambda \leq 50$  Å. A perhaps less direct way that would indicate the net migration direction is to measure the lattice constant of the Nb and Zr layers independently, keeping in mind that a change in the lattice constant parameter of one while the other stays constant would indicate that the changing lattice constant was brought about by a net gain of substitutional atoms since NbZr forms a substitutional solid solution.

A composition profile for  $\Lambda \geq 31$  Å can be established from satellites around nonzero lattice nodes; however, the satellite intensity around these nodes are affected by several factors which are very difficult to separate out especially in the case of coherent interfaces. In theory, central-node satellites can always be used to extract the composition modulation, but since the separation between the central-node and the  $L$ th satellite in reciprocal space is  $\pm L/\Lambda$  it is often not possible (when  $\Lambda$  is large) to separate the satellite intensity from that of the strong central node. With our diffractometer and sample geometry, the intensity of the central node extends out to approximately  $2\theta = 2^\circ$ , making any satellite below this value impossible to distinguish from the main beam. Although some of the higher-order satellites are above this cutoff, it is the lower-order satellites (or Fourier terms) that give the fundamental shape to the profile.

The widths of the main maxima are equal to those of the satellites, indicating that the modulation period does not vary substantially over the diffracting domain. The length of the diffracting domain along the growth direction increases as  $\Lambda$  decreases. A possible explanation for this increasing in the planar correlation along the growth direction is that the interfaces are becoming broader and more of the constituents exist in a solid solution at the interface. This increase in the amount of solid solution also causes a decrease in the amplitude of the composition wave, as evidenced by the decreasing number of satellites for modulation wavelength near 31 Å.

When the two separate lattices form a coherent bcc lattice, the upper and the lower satellites diminish in intensity and eventually disappear within the sensitivity of our diffractometer. This is as expected, since at this point there is little or no interplanar modulation. Although the amplitude of the interplanar-spacing modulation wave has become small or zero, this does not necessarily mean that the sample is no longer chemically modulated. If the sample remains chemically modulated beyond this point, the form-factor—modulation amplitude along the growth direction will not be zero. It is this region, below  $\Lambda \leq 31$  Å, that the multilayer has formed a coherent lattice with some degree of chemical modulation. The scattering-factor modulation or chemical modulation of the coherent lattice does appear in low- $|\vec{q}|$  scans along the growth direction. Therefore, below  $\Lambda = 31$  Å only the zero-node satellites remain to establish the composition modulation and profile. The composition profiles were obtained with the use of these satellites. Longitudinal scans at small  $|\vec{q}|$  show at least one satellite down to  $\Lambda = 13$  Å [see Fig. 2(b)].

#### IV. SUPERCONDUCTIVITY IN NbZr MULTILAYERS

Metallic multilayers of Nb and Zr provide an ideal system for studying the proximity effect between ultrathin slabs of superconducting and normal metals. The proximity effect is seen in the critical temperature of an  $N/S$  layer, as the relative thickness is varied. The critical temperature of such a system,  $T_{cNS}$ , falls in the range  $T_{cN} \leq T_{cNS} \leq T_{cS}$  where  $T_{cS}$  and  $T_{cN}$  are the superconducting transition temperatures for the superconductor and normal layers, respectively. Proximity-effect theory is well developed and has been applied to bilayers of superimposed thin films. Until recently, the application of the proximity-effect theory to multilayered thin films was not possible because the quality of the thin films was not sufficiently good to permit the coherence length to be greater than the modulation wavelength. With the higher-quality NbZr multilayers ranging from very small  $\Lambda$  to relatively large  $\Lambda$ , proximity effect theory valid to  $N/S$  layers much thinner than a coherence length can be tested.

It was initially proposed by Cooper,<sup>17</sup> and then modified slightly by de Gennes,<sup>18</sup> that in a layered superconductor in which the layer thicknesses are less than  $\xi$ , an effective attractive interaction could be used in the BCS equation to calculate the transition temperature. Assuming  $\xi > \Lambda$  with periodic boundaries and constant uniformity over each period in the NbZr multilayers, a single

period of the multilayer can be used to apply the Cooper—de Gennes model. In this work the model is extended to include a third layer at the interface of the  $N$  and  $S$  layers; therefore the model will be of the form Nb/NbZr/Zr. The effective attractive interaction for the trilayer is

$$[N(0)V]_{\text{eff}} = \frac{N_{\text{Nb}}^2 V_{\text{Nb}} d_{\text{Nb}} + N_{\text{Zr}}^2 V_{\text{Zr}} d_{\text{Zr}} + N_i^2 V_i d_i}{N_{\text{Nb}} d_{\text{Nb}} + N_{\text{Zr}} d_{\text{Zr}} + N_i d_i}, \quad (7)$$

where  $d_{\text{Nb}}$ ,  $d_{\text{Zr}}$ , and  $d_i$  are the thicknesses of the Nb, Zr, and the interface layers, respectively, and  $\Lambda = d_i + d_{\text{Nb}} + d_{\text{Zr}}$ .

When the individual layers are thin, such that the coherence length extends over many periods, this model can be applied to the NbZr multilayers. The behavior or the transition temperature in NbCu has also been explained within the Cooper limit; however, for those samples the interface was assumed to be infinitely sharp.<sup>19,20</sup> In applying this model it is assumed that the coherence length does extend over at least several periods of modulation and that the layers are alternately deposited fast enough to prevent interface oxide layers from forming. An asymmetry factor  $R = d_{\text{Nb}}/d_{\text{Zr}}$  is also added to allow for varying Nb and Zr thicknesses. The effective attractive interaction as given by Eq. (7) can either increase or decrease as a function of  $\Lambda$ . To differentiate between these behaviors we derive from Eq. (7) the function

$$f(N_{\text{Nb,Zr}}, V_{\text{Nb,Zr}}) = \frac{N_{\text{Nb}}^2 V_{\text{Nb}} + N_{\text{Zr}}^2 V_{\text{Zr}}}{N_{\text{Nb}} + N_{\text{Zr}}} \quad (8)$$

for  $R = 1.0$ , and compare its relative magnitude with  $N_i V_i$ , the attractive interaction for the interface layer. Assuming that  $N_i V_i$  is independent of  $\Lambda$ , when  $f(N_{\text{Nb,Zr}}, V_{\text{Nb,Zr}}) > N_i V_i$ , the effective attractive interaction, increases as  $\Lambda$  increases, and when  $f(N_{\text{Nb,Zr}}, V_{\text{Nb,Zr}}) < N_i V_i$ , it will decrease as  $\Lambda$  increases. It is interesting to note that, within the model,  $d_i$  does not play a part in determining which behavior is followed. Once  $[N(0)V]_{\text{eff}}$  is obtained  $T_{cNS}$  is calculated from the BCS equation,

$$T_{cNS} = \frac{\Theta_D}{1.45} \exp \left[ \frac{-1}{[N(0)V]_{\text{eff}}} \right], \quad (9)$$

where  $\Theta_D$  is the Debye temperature of the trilayer.

The critical temperatures of the NbZr multilayers were measured using an inductive technique in which multiple  $T_c$ 's could be detected. Measurements down to 3 K showed that every sample had only one transition approximately 0.1 K wide for  $\Lambda < 170$  Å and less than 0.2 K wide for  $\Lambda \geq 170$  Å. The critical temperature typically decreases as  $\Lambda$  increases (Fig. 4). This decrease is exponential up to about 100 Å and then almost linear up to  $\Lambda = 200$  Å. As  $\Lambda \rightarrow 0$  Å, the reported  $T_c$  of 9.7 K for the 50 at. % solid solution is obtained. The critical temperature changes smoothly through the Zr structural transition with no discontinuity or increase in the width of the critical temperature.

Two 0.5- $\mu\text{m}$  films, one of Nb and the other of Zr, were made under identical conditions of pressure and sputtering rates to determine a lower limit for the as-deposited criti-

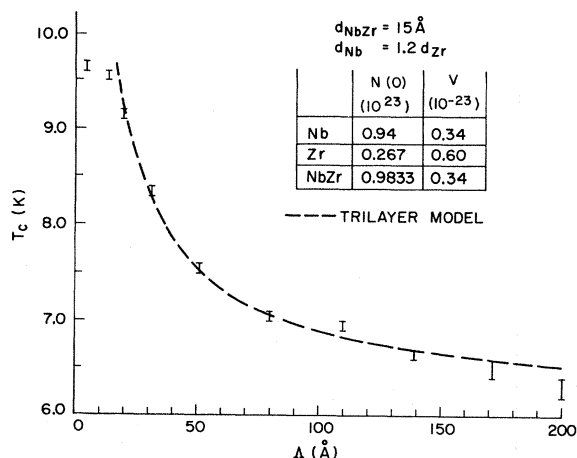


FIG. 4. Critical temperatures vs modulation wavelength showing narrow transition widths for all samples. The dotted curve is the calculated transition temperature for a trilayer model in the Cooper limit. At  $\Lambda \geq 100$  Å the modulation period is becoming comparable to the coherence length.

cal temperature for thick films. These critical temperatures are judged to be the lower limit because with only one sputtering source being used and the sample being rotated such that it spends 75% of its time out of the deposition beam, more impurities are incorporated in the film than in the preparation of the multilayer. Critical temperatures of the two samples made in this fashion were 8.2 K for Nb and 0.7 K for Zr.

The bulk electronic parameters  $N(0)$  and  $V$  for Nb and Zr were used in the calculation for the Nb and Zr layers. The interface layer was assumed to have a composition of  $\text{Nb}_{0.5}\text{Zr}_{0.5}$ . The pairing potential  $V_{\text{NbZr}}$  for the  $\text{Nb}_{0.5}\text{Zr}_{0.5}$  layer is assumed to be equal to  $V_{\text{Nb}}$ , that for pure Nb, and the density of states  $N_{\text{NbZr}}(0)$  calculated using the reported  $T_c$  for this concentration and Eq. (8). These values for the electronic parameters of the layers meet the condition that  $f(N_{\text{Nb,Zr}}, V_{\text{Nb,Zr}}) < N_{\text{NbZr}} V_{\text{NbZr}}$ . The Debye temperature used is the average of bulk Nb and Zr. With these values fixed the model was applied to the experimental  $T_{cNS}$  curve, and  $d_i = d_{\text{Nb}_{0.5}\text{Zr}_{0.5}}$ , the thickness of the interfacial alloy, and  $R$ , the asymmetry factor, varied independently to obtain the best fit. These values prove to be  $d_{\text{Nb}_{0.5}\text{Zr}_{0.5}} = 15$  Å and  $R = 1.2$ , and were used over the entire range of  $\Lambda$ . The model diverges and no longer applies when  $\Lambda < 19$  Å;  $T_c$  then approaches 9.7 K, which is the value for the  $\text{Nb}_{0.5}\text{Zr}_{0.5}$  solid solution.

The critical fields of the NbZr multilayers were not measured so the coherence lengths have not been determined; however, the Cooper limit  $\xi > \Lambda$  must apply in the small- $\Lambda$  region. Upon examination of the data and theoretical curve there is a functional difference at about  $\Lambda = 100$  Å which suggests that  $\xi$  is about 100 Å. If  $\xi \approx 100$  Å and  $\Lambda = 100$  Å, then  $\xi$  extends over one period, whereas  $d_{\text{Nb}} \approx d_{\text{Zr}} \approx 50$  Å and  $T_{cNS}$  would be reduced drastically from that of Nb. There is also evidence from the x-ray scattering that the interfaces are sharper, therefore causing  $d_{\text{Nb}_{0.5}\text{Zr}_{0.5}}$  to be smaller in this  $\Lambda$  region and

contributing to the adverse effect of  $T_{cNS}$ . A strong proximity effect is expected in the Nb, at least until  $d_{\text{Nb}} > \xi$ . The transition of the last two samples with  $\Lambda$  of 171 and 200 Å have broader transitions than the smaller  $\Lambda$  samples. This broadening of the transition infers that there are material inhomogeneities over distances comparable to  $\xi$ . Unfortunately, there is no data above  $\Lambda = 200$  Å to show a positive slope in the curve, but nevertheless the curve must eventually break into Zr and Nb branches and approach the bulk values of each.

## V. CONCLUSION

Multilayers of NbZr can be sputtered onto unheated substrates to form coherent interfaces with planar correlations over relatively large distances. The Zr undergoes a phase transition to become bcc with the same lattice constant as the Nb to form a coherent interface. The Zr phase transition is driven by the diffusion of Nb into the Zr layer. For modulation wavelengths below 100 Å, interdiffusion occurs significantly, reducing the multilayer to a near-sinusoidal modulated composition. There is evidence that this interdiffusion is slightly preferential such that Zr diffuses more into Nb. We could find no bulk diffusion data for Nb into Zr or Zr into Nb to compare with our results.

The small modulation wavelength samples have demonstrated that a composition modulation (although weak) can be maintained down to individual layer thicknesses of 3 or 4 atomic layers for systems that form disordered solid solutions. These samples also show clearly that after the nonzero-node satellites have become unresolvable or have disappeared there remains a composition modulation, even for such as atoms as Zr and Nb.

The superconductivity fits well into a simple Cooper-limit proximity model which allows for an interface layer between Nb and Zr. The model predicts that  $T_c$  as a function of  $\Lambda$  decreases when the interaction potential for the interface region is more than the averaged interaction potentials of Nb and Zr. This behavior is observed for NbZr multilayers. The smooth variation of  $T_c$  as a function of  $\Lambda$  while Zr is changing from hcp to bcc indicates that there is no significant difference in the density of states at the Fermi level between the two isomorphs.

## ACKNOWLEDGMENTS

We wish to acknowledge the preliminary studies on NbZr multilayers made by T. W. Barbee, Jr., in which the high degree of texture was first observed. We also wish to thank T. Claeson, D. B. McWhan, and J. Boyce for many rewarding discussions. One of us (W.P.L.) wishes to acknowledge support from the AT&T Bell Laboratories Research Fellows Program. This work was supported by the National Science Foundation—Materials Research Laboratories Program through the Center for Materials Research at Stanford University and the U. S. Air Force Office of Scientific Research under Contract No. F49620-82-C0014.

- <sup>1</sup>E. M. Gyorgy, D. B. McWhan, J. F. Dillon, Jr., L. R. Walker, and J. V. Waszczak, *Phys. Rev. B* **25**, 6739 (1982).
- <sup>2</sup>W. P. Lowe, T. W. Barbee, T. H. Geballe, and D. B. McWhan, *Phys. Rev. B* **24**, 6193 (1981).
- <sup>3</sup>I. K. Schuller, *Phys. Rev. Lett.* **44**, 1597 (1980).
- <sup>4</sup>S. M. Durbin, J. E. Cunningham, M. E. Mochel, and C. P. Flynn, *J. Phys. F* **11**, L223 (1981).
- <sup>5</sup>G. Hertel, D. B. McWhan, and J. M. Rowell, in *The Tunneling Density of States of Nb/Ta Superlattices, Superconductivity in d- and f- Band Metals 1982*, edited by W. Buckel and W. Weber (Kernforschungszentrum Karlsruhe GmbH, Karlsruhe, West Germany, 1982).
- <sup>6</sup>J. Q. Zheng, J. B. Ketterson, C. M. Falco, and I. K. Schuller, *Physica* **108B&C**, 945 (1981).
- <sup>7</sup>T. Claeson, J. B. Boyce, W. P. Lowe, and T. H. Geballe, following paper, *Phys. Rev. B* **29**, 4969 (1984).
- <sup>8</sup>F. Gompf, W. Richter, and W. Weber, *Physica* **108B**, 1337 (1981).
- <sup>9</sup>E. L. Wolf, R. J. Noer, and G. B. Arnold, *J. Low Temp. Phys.* **40**, 419 (1980).
- <sup>10</sup>S. L. Sass, *J. Less Comm. Metals* **28**, 157 (1972).
- <sup>11</sup>B. A. Hatt and J. A. Roberts, *Acta Metall.* **8**, 575 (1960).
- <sup>12</sup>R. Pynn, W. G. Stirling, M. Ishikawa, and E. Walker, *Solid State Commun.* **32**, 767 (1979).
- <sup>13</sup>T. W. Barbee, Jr. and D. Keith, Stanford University Synchrotron Radiation Laboratory (Stanford, Ca.) Report No. 78-04 (1978) (unpublished).
- <sup>14</sup>B. D. Cullity, *Elements of X-Ray Diffraction* (Addison-Wesley, Menlo Park, California, 1978).
- <sup>15</sup>D. de Fontaine, in *Local Atomic Arrangements Studied by X-ray Diffraction, Proceedings of the Metallurgical Society Conferences*, edited by J. B. Cohen and J. E. Hilliard (Gordon and Breach, New York, 1966), p. 51.
- <sup>16</sup>W. B. Pearson, *A Handbook of Lattice Spacings and Structures of Metals and Alloys—2* (Pergamon, New York, 1967).
- <sup>17</sup>L. N. Cooper, *Phys. Rev. Lett.* **6**, 689 (1961).
- <sup>18</sup>P. G. de Gennes, *Rev. Mod. Phys.* **36**, 225 (1964).
- <sup>19</sup>I. K. Schuller and C. M. Falco, in *Layered Ultrathin Coherent Structures*, Proceedings of the International Conference on Inhomogeneous Superconductors, edited by D. U. Gubser, T. L. Francavilla, J. R. Leibowitz, and S. A. Wolf (AIP, New York, 1979), pp. 197–202.
- <sup>20</sup>I. Banerjee, Q. S. Yang, C. M. Falco, and I. K. Schuller, in Superconductivity of NbCu Superlattices [*Solid State Commun.* **41**, 805 (1982)].